Elucidation of Switching Mechanisms in Memristive Junctions Integrating a Iron(II)-Ter Pyridine Diazoted Complex

Camille Jubert Tomasso, Thomas Petenzi, Anna Tidu, Rassen Boukraa, Sofia Russi, Giorgio Mattana, Christelle Gautier, Tony Breton, Ivan Lucas, Hubert Perrot, et al.

ADVANCED ELECTRONIC MATERIALS Open Access
www.advelectronicmat.de

Elucidation of Switching Mechanisms in Memristive Junctions Integrating a Iron(II)-Ter Pyridine Diazoted Complex

Camille Jubert Tomasso, Thomas Petenzi, Anna Tidu, Rassen Boukraa, Sofia Russi, Giorgio Mattana, Christelle Gautier, Tony Breton, Ivan T. Lucas, Hubert Perrot, and Laure Fillaud**

An original way of elaborating vertical metal/molecules/metal memristive junctions through diazonium electrografting of the organic layer and inkjet-printed top electrodes is reported here. The molecule of interest is a Fe^{II} coordination complex with ter-pyridine ligands, having a diazonium anchoring group. The resulting junction exhibits a memristive behavior characterized by a high ON/OFF ratio and plasticity property. Through the application of advanced techniques such as UV–vis and Raman time-resolved spectroelectrochemistry, the study demonstrates the significant role of switchable azo bonds derived from diazo electrografting in memristive behavior.

1. Introduction

Memristors are two-path compact devices able to store and process information thanks to a resistive switch occurring in their active layer.[1–3] These non-volatile memories are relevant components for new computing generations, based on neuromorphic circuit architectures, in which they mimic synapses where a neuron can be connected to 10000 synapses.[4,5] This technology is promising for improving computing calculations in a confined space while minimizing memory power consumption.

Among the myriad materials of interest in this field, coordination complexes are good candidates to develop memristive devices. They are described as switching materials, stable in various controllable resistive states.[6–11] Switching events in these complex films are usually attributed to charge transfer or redox mechanisms. Overall, complexes are well suitable because the chemical tuning of organic ligand functions is easily processible by synthesis. In addition, their redox properties may enable access to more than two resistive states for multi-unary coding junctions.[12,13] For instance, it has been shown for cobalt, rhodium, and ruthenium complexes that their ligand azo bond moieties are responsible for a resistive switch.[9,10,14–16] These studied devices were made by spin coating of the molecular layers on ITO support. Then, the top electrodes were thermally evaporated. Nevertheless, this fabrication approach limits the layer thickness and localization control which disadvantages device design and miniaturization. Other limitations of these complexes are the cost of metals and their accessibility.

In light of these considerations, our work focuses on a new Fe complex with two ter-pyridine derivatives as ligands, one of which has a diazonium anchoring group at its end (**Figure 1**). Iron, a non-expensive metal having redox activity, has already exhibited memory behavior in ferrocene complex polymers.[17,18] Ter-pyridine (tPy) ligands enable electronic conduction due to their aromaticity. The diazonium grafting approach offers the clear advantage of controlling thickness deposition by electroreduction of molecules, forming a covalent bond that links the bottom electrode by a covalent bond.[19–22] As evidenced by D. Bélanger and later J. Pinson, films formed using this technique generally incorporate a variable proportion of azo bridges between molecules, a formation mechanism that remains unclear.[20,23–25] P. A. Brooksby and A. J. Downard have observed the electrochemical inactivity of those azo bonds in a nitroazobenzene film,[26] even though recent studies have suggested their redox

C. Jubert Tomasso, T. Petenzi, A. Tidu, S. Russi, H. Perrot, L. Fillaud
LISE
Sorbonne Université
Paris 75005, France
E-mail: camille.jubert@gmail.com; laure.fillaud@sorbonne-universite.fr
R. Boukraa, G. Mattana
Université Paris Cité, ITODYS, CNRS
UMR 7086
15 rue J.-A. de Baïf, Paris F-75013, France
C. Gautier, T. Breton
Moltech Anjou
Université d'Angers
Angers 49100, France
I. T. Lucas
IMN
Nantes Université
Nantes 44300, France

The ORCID identification number(s) for the author(s) of this article can be found under https://doi.org/10.1002/aelm.202400350

DOI: 10.1002/aelm.202400350

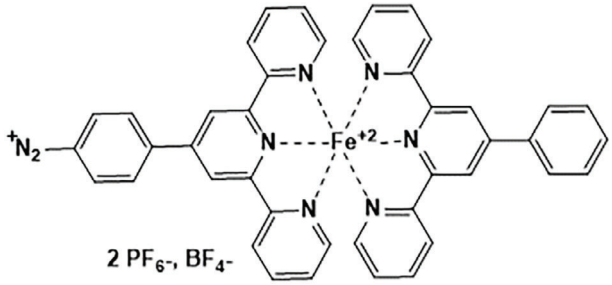

Figure 1. Structure of the studied Fe complex.

properties, potentially contributing to resistive switching behavior in the films.[13,27] However, the study of chemical and electronic switching mechanisms in molecular layers is still challenging. Thus, this work aims to demonstrate the electroactivity of azo bridges in Fe complex films and to correlate it with the memory behavior of the complex embedded in metal/molecules/metal junctions.

The ambition of this work is to provide new characterization strategies to promote device's electronic mechanisms understanding. For the deep investigation of the electrochemical behavior, a multiplex platform was specifically elaborated. This conceptual design has been proved to allow direct advanced characterizations by AFM, in situ Raman spectroscopy, and i-V measurements to be performed. To better understand the memristive mechanisms, the complex films were also investigated by real-time UV–vis spectroelectrochemistry to attribute absorption variations to redox events and Raman signatures have been followed under electrochemical conditions to understand redox reactions involved in molecular layers.

2. Film Controlled Electrografting

2.1. Electrochemical Investigations

$[Fe(\Phi tPy)(N_2{}^+\Phi tPy)(PF_6{}^-)_2(BF_4{}^-)]$ grafting was achieved by chronoamperometry (CA) as described in the experimental part. **Figure 2** presents the electroactivity of the layer formed by the reduction of the diazonium. Fe^{II}/Fe^{III} redox couple is observable at +1.2 V versus Ag/AgCl and tPy^0/tPy^{+1} couple appears as two waves at −1.1 and −1.2 V versus Ag/AgCl due to the ligand's asymmetry in the complex. The surface concentration of the complex grafted was estimated to be 8.29×10^{-9} mol•cm^{-2} by integration of the charge exchanged during the metal redox process. The origin of the two pre-peaks in oxidation at +0.9 V and in reduction at −0.5 V versus Ag/AgCl remains to be identified. However, under repetitive cycling in the oxidation window (i.e., 0 V to +1.3 V), the oxidative pre-peak only appears at the first scan. Similar pre-peaks have already been observed for Fe^{2+} and Ru^{2+} complexes with pyridine derivatives as ligands.[28,29] In the literature it was hypothesized they could result from charge trapping in the film.[29] Another possibility is that they come from redox activity of the azo bonds formed during diazonium electrografting.[13] A part of our work aims to elucidate the pre-peaks origin.

As the grafting process succeeded, the controled deposition using chloranil (ChA) as a redox inhibitor was investigated (Cf. Figure 2).[30] It was found that the film current response decreases while increasing the inhibitor amount, thus, indicating that the film thickness/quantity or active electrochemical sites decrease. By varying the ChA concentration, thickness-controled layers can be obtained and characterized by integrating the exchanged charge during the redox process Fe^{II}/Fe^{III}. Taking as a reference the surface concentration of the complex obtained from a compact self-assembled monolayer of its thiol derivative (i.e., $[Fe(SH\Phi tPy)(\Phi tPy)(PF_6)_2]$ 9.2×10^{-11} mol•cm^{-2}) (Cf Figure S1, Supporting Information), it was found that a near-monolayer of the complex is reached for 0.35 eq. of ChA (i.e., 4.14×10^{-10} mol•cm^{-2}). Interestingly, the oxidation and reduction pre-peaks were not observed for the thinnest layers prepared.

To confirm the inhibitor efficiency, grafting was then followed by EQCM with 0 and 0.35 eq. of ChA (Figure S2, Supporting Information). The mass of the film grafted with ChA was found much lower than the mass of the multilayer obtained without ChA (i.e., 2.2 vs 9.63×10^{-10} mol•cm^{-2}), which is consistent with the electrochemical measurements.

2.2. X-Ray Photoelectron Spectra (XPS) Characterization

Films obtained through the reduction by cyclic voltammetry (CV) of the diazotized Fe complex without and with chloranil in the deposition solution were analyzed by X-ray photoelectron spectroscopy. Integration of the high-resolution N1s spectra showed that the use of chloranil as a redox inhibitor led to a 35% drop in the nitrogen concentration (Figures S3 and S4, Supporting Information). Considering that the nitrogen atoms mainly come from the pyridine rings, this drop can be assimilated to an equivalent decrease in the Fe complex surface concentration. Concomitantly, the large signal increase observed on the Au 4f core level spectrum when the grafting is performed in the presence of chloranil indicates that the gold substrate represents a larger proportion of the probed material and is thus consistent with a drastic decrease of the layer thickness.

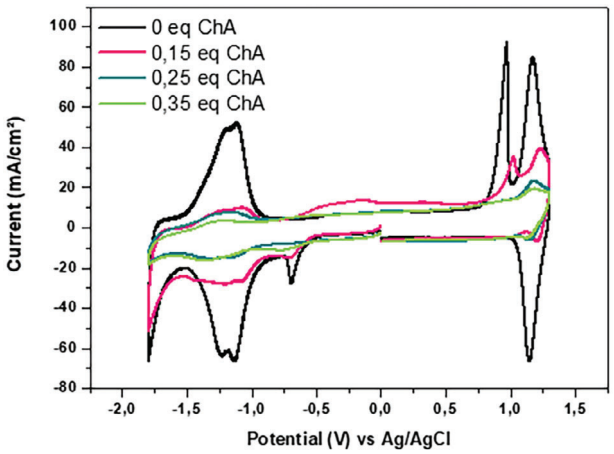

Figure 2. Electroactivity of Fe(II) complex films grafted on glassy carbon (GC) under Ar with different amounts of ChA inhibitor between [−1.8; 1.3] V versus Ag/AgCl (in ACN : nBu_4NPF_6, 100 mV.s^{-1}).

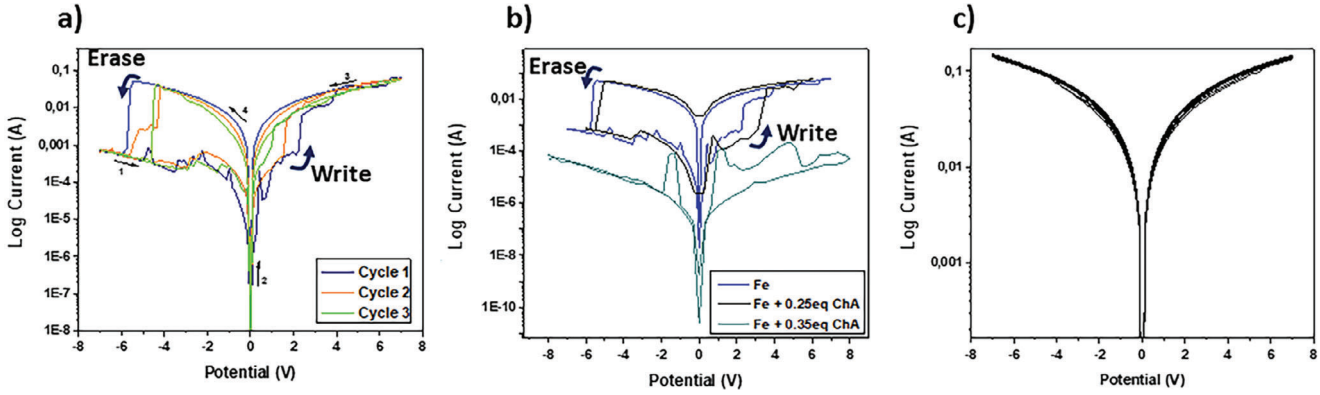

Figure 3. i-V characteristic of a) Au/complex/Au junction made of [Fe(N_2^+ΦtPy)(ΦtPy)] grafted by CV (3 cycles on the range [−0.4, 0] V vs Ag/AgCl) b) and junctions made by complex grafting with 0, 0.25, and 0.35 eq ChA. c) Au/complex/Au junction of a [Fe(SHΦtPy)(ΦtPy)] SAM.

3. Device Investigation

3.1. Junction Evaluation

The multilayer complex film, obtained by CV, was integrated into a Au/Fe film/Au multiplex platform to study its resistive switch behavior. The junction was polarized from −6 V to +6 V, a switch ON to a more conductive state has been recorded at ≈2.5 V then, the switch OFF occurred at ≈−5 V (**Figure** 3a). The ON current is up to 5×10^{-2} A and the ratio of 100 between both ON and OFF states corresponds to the targeted standards of a good memristor.[31] ON/OFF switches appear at smaller potentials while cycling the memristor, disclosing its plasticity once integrated into a network. This kind of learning ability has been observed in previous work on a memristor integrating a Fe^{II} complex with bipyridine ligands.[32] A Au/Fe film/Ag junction has also been made (Cf Figure S7, Supporting Information) and exhibited a memristive behavior for more than 40 cycles. Both types of junctions show unique switching characteristics indicating that the top electrode's material is not at the origin of the memristive behavior, so filamentary and charge transfer mechanisms can be ruled out.[1,2] Few studies on coordination complexes reported switching coming from azo bridges of the ligands.[13,27] Thus, we speculated that the mechanism could come from the redox activity of the metal and azo bridges formed during the complex grafting.

I–V curves obtained from junctions made with a Fe complex layer controlled by ChA are presented in Figure 3b. The junction integrating the film grafted with 0.25 eq of ChA exhibits a switch similar to the junction made from the thick film, without ChA. When the junction thickness is lowered to a two-layer film by increasing the ChA concentration to 0.35 eq., the device shows a current jump but has no stable memory effect. The amount of azo bonds in this thin film is probably too small to provide memristive behavior. As a comparison, Figure 3c shows the i–V curve recorded for the Au/complex/Au junction integrating the self-assembled monolayer made with [Fe(SHΦtPy)(ΦtPy)(PF_6)$_2$]. As expected for such a thin organic layer, the junction is short-circuited because the printing ink for the top electrode crossed the monolayer.

The present paper demonstrates the suitability of printing techniques for the fabrication of electrodes in memristive devices. Even if the substrates used in this work were rigid silicon wafers, one can actually think of using flexible, plastic substrates, provided that they are compatible with the thermal treatment necessary to sinter the ink (such as Kapton or other types of polyimides). Moreover, not only could these techniques be used for the fabrication of the top electrodes but also for the bottom ones. The use of such substrates could indeed lead toward the fabrication of large-area arrays of devices, provided that the following issue is taken into account: the chemical compatibility between the printed bottom electrodes and the electrochemical process necessary to graft the complex onto them. A work previously published by some of the authors seems to suggest that such a grafting may be possible, as inkjet-printed Au electrodes have similar electrochemical behavior as thermally evaporated ones.[33] As for the design aspect of device arrays on large-area, plastic substrates, care should be taken when dealing with issues such as flexibility: adhesion between electrodes and substrates becomes crucial, and dedicated protocols should be taken to improve it (UV–ozone or plasma treatments or surface functionalization prior to electrodes deposition).

To elucidate switching mechanisms, redox properties of the complex thick film were further investigated by UV–vis absorption and Raman spectroscopies combined with electrochemistry.

4. Advanced and Coupled Electrochemical Investigations

4.1. UV–Vis Absorption Spectroelectrochemistry (ASEC)

The complex was first studied in solution by spectroelectrochemistry (1 mM in electrolytic solution, GC electrode) using a diazonium-free structure in order to prevent any grafting. The solution was probed by setting the electrode close to the optical fibers (typically 50 μM) to obtain a diffusion-free voltammetric response analyzed in thin layer conditions.

The obtained voltammogram shows the reversible oxidation of [Fe(ΦtPy)$_2$] into [Fe(ΦtPy)$_2$]$^{+1}$ at +1 V (**Figure** 4a,b). The corresponding voltabsorptogram shows a negative absorption band centered at 580 nm, corresponding to the extinction of the metal-to-ligands charge transfer (MLCT) band in its initial redox state (Figure 4c). This band is in good agreement with the UV–vis spectrum of [Fe(ΦtPy)$_2$] presented in Figure S9 (Supporting

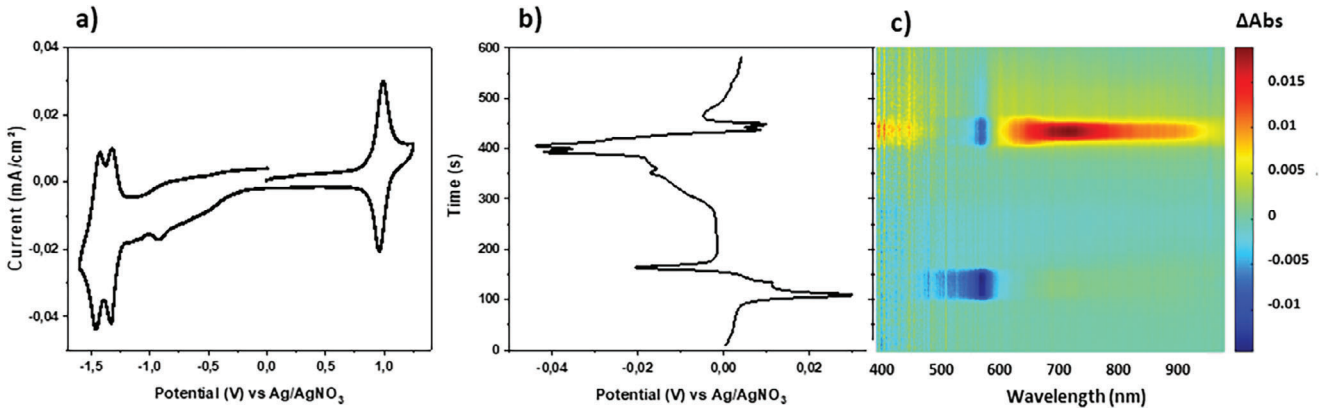

Figure 4. ASEC of $[Fe(\Phi tPy)_2]$ complex measured with a GC electrode. a) CV of the complex (in ACN: nBu_4NPF_6, [−1.6; +1.3] V vs $Ag/AgNO_3$, 10 $mV.^{-1}$) and b) Current compared to ΔAbs/dt at 580 nm plotted as a function of time. c) corresponding voltabsorptogram.

Information) (maximum at 570 nm). Two reversible processes appear at −1.1 and −1.2 V versus $Ag/AgNO_3$. In this potential window, a negative absorption band centered at 580 nm (MLCT band) and a large positive absorption band centered at 750 nm (reduced ligands) are observed.

The deposition of the complex carrying a diazonium function $[Fe(\Phi tPy)(N_2{}^+\Phi tPy)(PF_6{}^-)_2\ (BF_4{}^-)]$ was then carried out by CA in the absence of chloranil (for 300 sec, at −0.4 V vs $Ag/AgNO_3$). The multilayered complex obtained was probed by UV–vis spectroelectrochemistry upon cycling (**Figure 5**). The CV procedure was preceded by a short-fixed potential step at 0 V for which no redox process occurs to establish a ΔAbs reference value. The voltabsorptogram clearly shows appearing (red) and disappearing (blue) species depending on the redox activity.[34] Negative ΔAbs signals are observed at 600 nm during the Fe^{II}/Fe^{III} reversible oxidation process and during the reversible reduction of the ligands (Figure 5a,b). These ΔAbs variations are attributed to the disappearance of the charge transfer from the metal to the ligand (MLCT) band upon oxidation and reduction of the Fe complex. The positive ΔAbs signals at 900 nm are associated with the appearance of reduced tPy. In addition, a positive signal appears at 580 nm, concomitantly to the oxidative pre-peak at +0.9 V (corresponding to 20 s). This positive Δabs signal persists on the spectrum during the negative scan and is only lost when the reductive pre-peak rises at −0.5 V (corresponding to 47 s), indicating a species formation and disappearance.

Furthermore, repetitive cycling on the oxidation region of the complex is presented in Figure 5c,d. The pre-peak at +0.9 V is lost over the cycles whereas the signal at 580 nm is preserved, demonstrating that the species formed during the first oxidation is still present once the complex is reduced. This observation highlights the interdependence of the reducing and oxidizing pre-peaks.

Katz and coworkers reported the redox activity of azo bonds by comparing UV–vis spectra of chemically reduced azo (HN-NH) to electrochemically reduced azo of a ruthenium complex.[35] They also studied a rhenium complex with a ligand having an azo bridge by UV–vis spectroscopy under electrochemical polarization at −316 and −800 mV and established that the neutral azo (N═N) has absorption bands at 250, 300, and 400 nm, the mono-reduced form (HN—N═) absorbs at 500, 600, and 800 nm and the doubly-reduced azo (HN-NH) absorbs at 250, 300, 400, and 700nm.[27]

In our case, the absorption band appearing at 580 nm, associated with the pre-peaks, is thus suspected to arise from azo bonds formed in the film during the complex grafting. Moreover, the absorption variation during cycling demonstrates azo redox properties.

As evidenced by following Raman results, azo bonds are present in both neutral and doubly-reduced forms (N═N and HN-NH) in the film before any electrochemical measurements. This means that the doubly-reduced form is oxidized at +0.9 V to the mono-reduced azo and reveals the band at 580 nm. This form remains visible until its reduction at −0.5 V.

4.2. Raman Spectroscopy Coupled to Electrochemistry

Raman signature of a thick complex film grafted on carbon was recorded simultaneously with its CV characterization (**Figure 6**). Spectra collected at 0, +1, +1.3 then −0.3 V during the first cycle are presented in Figure 6b. For spectra collected at 0 and +1 V, two peaks are visible at 1557 and 1600 cm^{-1}. On the spectrum measured at +1.3 V, a third peak appears at 1577 cm^{-1}, which disappears when cycling at −0 .3V.

A similar study has already been conducted by Goswami et al.[8] The authors studied by Raman spectroscopy coupled to i-V characterization a ruthenium complex having azo bridges integrated into a transparent junction made on ITO. Three bands were observed at 1275, 1313, and 1365 cm^{-1}, corresponding to azo bonds in different oxidation states, which appear or disappear depending on the device polarization. For a smaller molecule, two azo bands are reported between 1400 and 1452 cm^{-1}. Herein, the peaks at 1557, 1577, and 1600 cm^{-1} are shifted but they can be attributed to azo stretching. The neutral (N═N) and doubly-reduced azo (HN-NH) are initially present in the film, their corresponding bands are respectively located at 1557 and 1600 cm^{-1}. After the pre-peak at +1 V, the mono-reduced azo (HN—N═) appears from the doubly-reduced species oxidation and is visible at 1577 cm^{-1}. The mono-reduced azo is then reduced to (HN-NH) form while cycling up to −0.3 V but this was observed only for

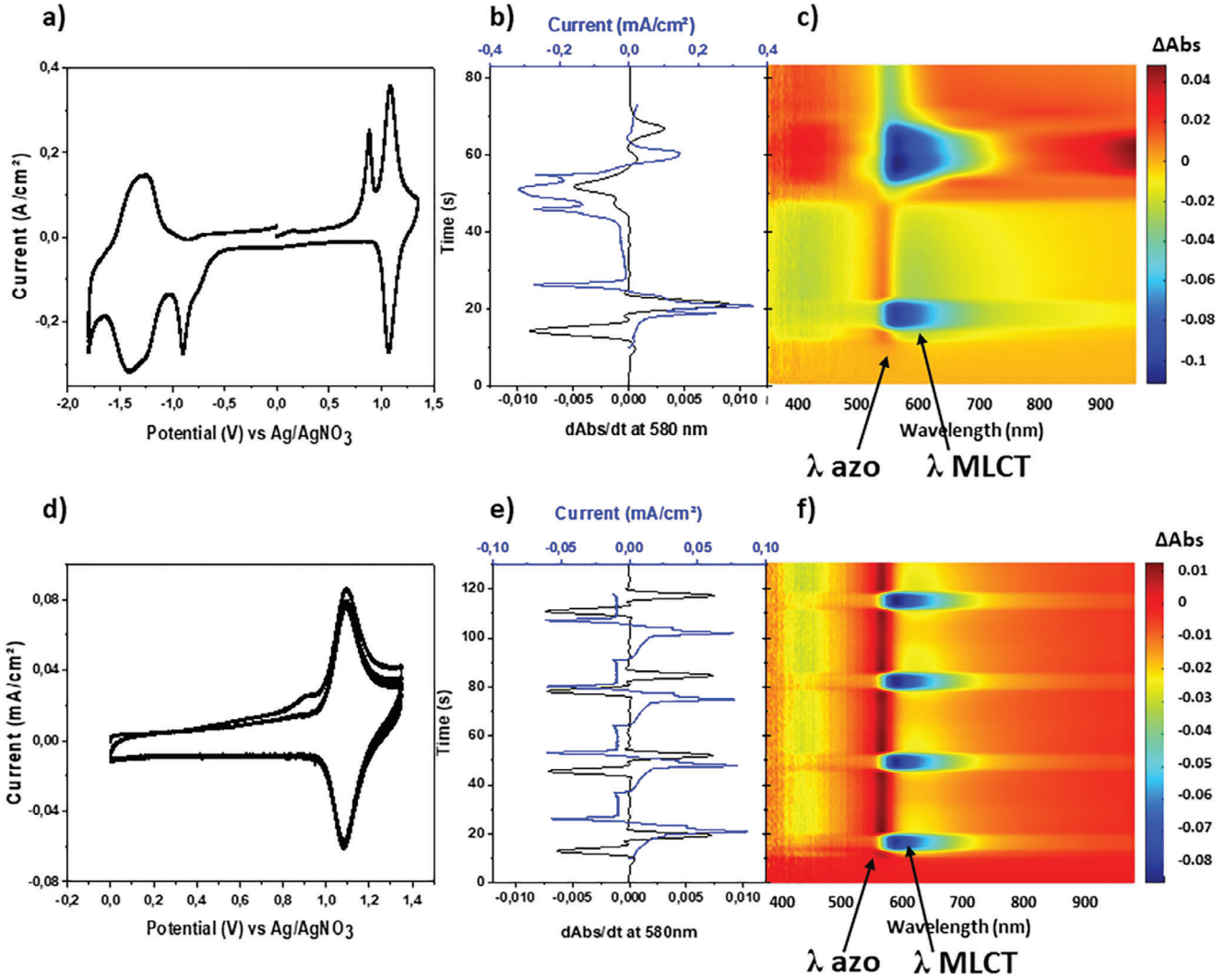

Figure 5. ASEC of [Fe(ΦtPy)(N_2^+ΦtPy)] film on GC in ACN electrolyte. a) CV of the complex (in ACN: nBu_4NPF_6, [−1.8; +1.3] V vs $Ag/AgNO_3$, 100 $mV.s^{-1}$). b) CV compared to dAbs/dt plotted in function of time and c) corresponding voltabsorptogram. d) CV at positive potential (in ACN:nBu_4NPF_6, [0; +1.3] V vs $Ag/AgNO_3$, 100 $mV.s^{-1}$). e) Oxidative CV compared to dAbs/dt plotted in function of time and f) corresponding voltabsorptogram.

the first cycle of CV because the polarization was not negative enough.

The organic layer must be characterized at the solid state to be able to attribute the memristor resistive states to the different azo redox forms. The perspective is to build a transparent junction, as described by S. Goswami and coworkers.[8] The Raman signature of the azo bridges could then be monitored while cycling in potential the junction.

5. Conclusion

In this work on Fe complex, the formation of azo bonds during diazonium electrografting was evidenced by spectroscopic techniques. Their electroactivity was shown by UV–vis and Raman spectroscopy coupled to electrochemistry. The property of azo to be reversibly doubly reduced confers resistive switching behavior to junctions integrating the grafted Fe complex.

The memristor made with the Fe thick film exhibits promising performances. Writing and erasing potential are low and the ON/OFF ratio is large. Nevertheless, further research is needed to improve memristors endurance. In particular, film structures could be tuned by playing on azo bridges to study their impact on i–V curves.

6. Experimental Section

Materials: Reagent-grade solvents were purchased from VWR-Prolabo or Alfa Aesar. Benzaldehyde, 4-nitrobenzaldhyde, 2-acetylpyridin, palladium on carbon, hydrazine monohydrate potassium hydroxide, sodium hydroxide, iron (II) chloride tetrahydrate, ammonium hexafluorophosphate, nitrosyl tetrafluoroborate, and p-chloranil were purchased from Sigma–Aldrich or Alfa Aesar and used as received (>98%). N-doped silicon wafers 280 µm thick and with a resistivity between 0.002 and 0.009 Ω cm were purchased from Sil'tronix. Lab-made gold substrates (100 nm of

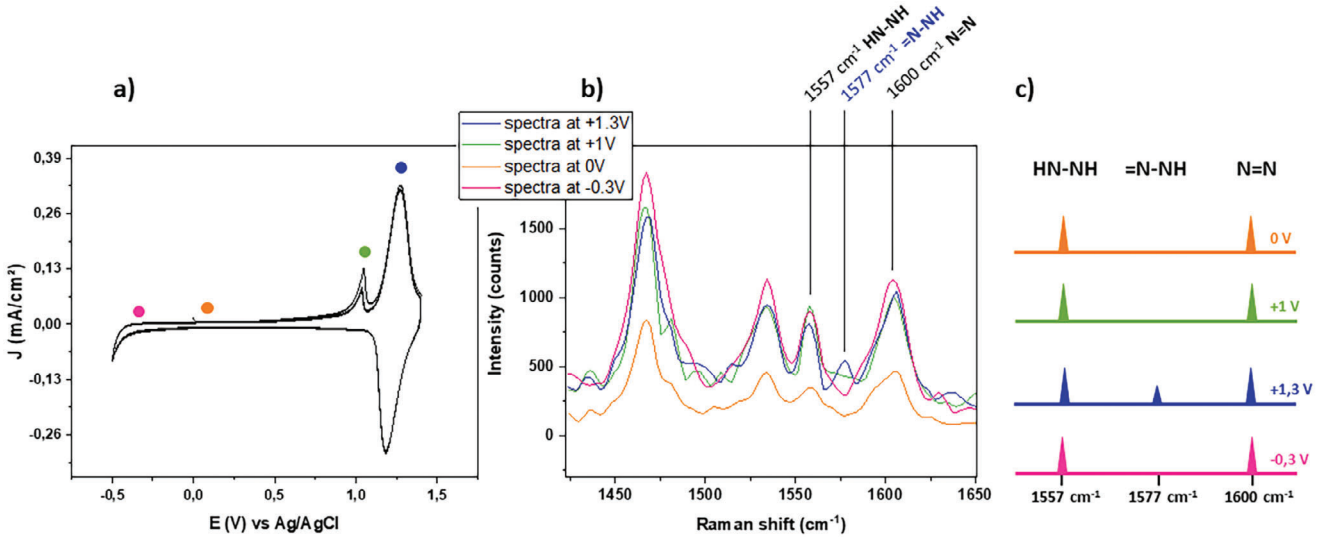

Figure 6. a) CV of a [Fe(ΦtPy)(N_2^+ΦtPy)] film in ACN (on GC, [-0.5, 1.4] V vs Ag/AgCl, at 100 mV.s^{-1}). b) Raman spectra recorded at -0.3; 0; +1 and +1.3 V versus Ag/AgCl simultaneously to the CV. c) Schematic view of the Raman signature evolution.

Au deposited onto mica) were used for the X-Ray Photoelectron Spectra experiments.

Ligands and Complexes Synthesis: The ligands 4′-(4R-Phenyl)-2,2′:6′,2″-terpyridine (RBtPy), where R can be H or N_2^+ were synthesized according to the procedure previously described.[30,36,37] Briefly, to a solution of the corresponding aldehyde in ethanol, 2-acetylpyridine and potassium hydroxide were successively added. An aqueous ammonia solution was then added and the reaction mixture was heated to reflux for 48 h. A precipitate appeared and was filtered, washed with diethyl ether, and dried over vacuum. Thus, the powders obtained (yield between 30 and 80%) were characterized by NMR and infrared spectroscopy. The asymmetric iron complexes were obtained in three steps (see SI). The first one consists of obtaining the complex [Fe(ΦtPy)$(Cl)_2(CH_3CH_2OH)$], then the ligand carrying the amine function was added to the reaction mixture. In the end, the complex [Fe(ΦtPy)$(NH_2ΦtPy)(PF_6^-)_2$] was obtained. The diazotization of the amine function was carried out in acetonitrile in the presence of nitrosyl tetrafluoroborate at −40 °C under an argon atmosphere as previously described in the literature.[38] The complex [Fe(N_2^+ΦtPy)(ΦtPy)$(PF_6^-)_2(BF_4^-)$] was finally isolated.

Electrochemical Experiments: All electrochemical experiments were conducted in a three-cell electrode, with tetrabutyl ammonium hexafluorophosphate (nBu_4NPF_6, 0.1 M) as a supporting electrolyte. Electrochemical reduction of diazonium salt (1 mM in electrolyte) was conducted under an argon atmosphere by cyclic voltammetry (3 cycles in the range [−0.4, 0] V vs Ag/AgCl) or chronoamperometry (at −0.4 V vs Ag/AgCl during 5 min). The layer thickness was controlled by the presence of chloranil as redox inhibitor whose concentration was adjusted from 0 to 0.35 equivalents.[30]

The electrochemical study of the formed layers was carried out in the electrolyte by cyclic voltammetry at a scanning rate of 100 mV•s^{-1}. All electrochemical experiments were conducted on a CHInstrument potentiostat (CHI240C) in a three-electrode cell, with homemade Ag/AgCl/KCl_{sat} as reference electrode, glassy carbon electrode (GC- diameter 3 mm) purchased from BAS Inc. or gold electrode (Au- diameter 3 mm) purchased from Origalys SA as working electrode, and a platinum grid as counter-electrode.

Electrochemical Quartz Crystal Microbalance (EQCM): Electrochemical quartz crystal microbalance (EQCM) measurements were performed with a lab-made EQCM connected to a Yokogawa TC110 frequency counter coupled to an Autolab PGSTAT100 potentiostat. An electrochemical closed cell incorporating a gold-coated quartz resonator (AWS Spain, 9 MHz, 14 mm Ti/Au) was used in a horizontal setup equipped with a platinum wire as counter electrode and an Ag/AgCl reference electrode. EQCM experiments were carried out to monitor the mass change of the electrode during the electrochemical reduction of the diazonium cation under the electrochemical modification conditions described above.[39] Gravimetric regime was validated using a Network Analyzer and by determining a dissipation factor evolution during the film elaboration. This change was compared to the change in the resonant frequency of our resonators.

Multiplex Platform Fabrication: *The bottom electrodes* were manufactured as follows. Silicon wafers were rinsed with acetone and isopropanol in an ultrasonic bath and dried under argon. The wafers were dehydrated on a hot plate (120 °C) for 10 min. The substrates were coated with AZ5214E resist, prebaked on a hot plate (110 °C, 1 min), and exposed to UV light for 1.8 s in low vacuum mode (Mask Aligner MJB4 by Süss Microtec; exposure: 12 mW•cm^{-2} at 365 nm). Reversal bake was done on a hot plate (120 °C, 2 min). The substrates were then flood-exposed for 1 min and afterward immersed into a standard developer MIF726 for 1 min; subsequently, they were rinsed in water for 1 min. Finally, thermal evaporation was performed (3 nm Cr, 100 nm Au). Then, the excess of gold was removed by lift-off, using an ultrasonic bath and acetone. The resulting electrodes consist of a 4 × 4 mm^2 square connected with two electrodes. These electrodes are 20 µm wide and 10 mm long and are spaced at 1.50 mm. The third one is not connected to the square in order to serve as a reference for the thickness measurements of the layer (**Figure 7a**).

Layer Deposition: The [Fe(ΦtPy)(N_2^+ΦtPy)$(PF_6^-)_2(BF_4^-)$] (1 mM) grafting on gold electrodes was achieved in an acetonitrile nBu_4NPF_6 0.1 M electrolyte by using cyclic voltammetry (3 cycles) between 0 and −0.4 V versus Ag/AgCl (Figure 7b).

Top Electrodes: They were manufactured as follows. Ag electrodes were printed using a Dimatix Fujifilm DMP-2800 printer with 10 pL drops cartridges and an inkjet-printable Ag nanoparticles-based ink (Sicrys I40TM-106, by Pv NanoCell, metal loading: 40% wt). Drop spacing was set at 20 µm, and the standard Dimatix Waveform was utilized. A sintering step (180 °C for 1 h) was applied after printing, to promote solvent evaporation and nanoparticles sintering. Ag top electrodes are ≈0.5 mm wide and 2.5 mm long. Au top electrodes were printed using an inkjet-printable Au nanoparticles-based ink (Novacentrix Metalon JG-124, metal loading: 25% wt). Deposition of Au electrodes was carried out using an ink-dispenser (Kelenn Technology DMD 100), using a 32 gauges needle. The printing speed was 200 mm.min^{-1} and the deposition pressure was from 2 to 5 kPa. A sintering step (200 °C for 30 min) was applied after printing. Au top electrodes are ≈0.5 mm wide and 18 mm long to contact

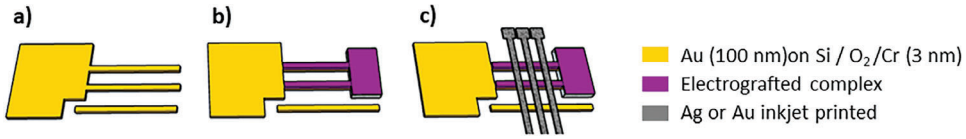

Figure 7. Devices fabrication a) gold bottom electrodes; b) organic thin layer deposition;c) inkjet-printed top electrodes.

three devices (Figure 7c). A picture of the elaborated multiplex platform is presented in Figures S5 and S6 (Supporting Information).

Current–Voltage Characterization: The current–voltage characteristics were measured by applying a voltage difference between bottom and top electrodes electrically connected with a lab-made tungsten tip fixed on a micromanipulator. The applied potential range was from −6 to 6 V with a potential step of 0.12 V. The current–voltage characteristics were measured using a source meter dual channel analyzer (Keithley2602B, Keithley Instruments, Germany).

Time-Resolved Spectroelectrochemistry (ASEC): Time-resolved spectroelectrochemistry measurements were performed by using an already-described lab-made bench designed by Levillain and coworkers (Cf. Figure S8, Supporting Information).[40] *Electrochemical measurements* were carried out by using a Biologic SP-150 potentiostat driven by EC-Lab software, with a platinum wire counter electrode and a $Ag/AgNO_3$ (10 mM) reference electrode. *Spectrophotometric measurements* were carried out in direct reflexing mode on the working electrode (glassy carbon) with a bench composed of different Princeton Instruments modules (light sources, optic fibers, monochromators, CCD spectroscopy camera, and software). For each data set, the reference intensity (Iref) was obtained by averaging the intensity of the first 10 measured frames. Consequently, absorbance variations (ΔAbs = − log10 (I/Iref)) and not absorbance values were monitored.

Time-Resolved Raman-Electrochemistry: Time-resolved SERS-electrochemistry measurements were performed by using a lab-made cell presented in Figure S10 (Supporting Information).

The Raman spectra were collected by using a Raman optical microscope (Horiba, LabRam Evolution HR800) equipped with 5 laser lines (473, 532, 594, 633, 785 nm) and a near-infrared sensitive CCD detector (Syncerity). The source used in this work is a 532 nm laser, at 1 or 2.5%. of intensity.

Electrochemical measurements were carried out by using a CHInstrument potentiostat (CHI240C), with a platinum grid counter electrode and an Ag/AgCl/KClsat reference electrode.

Gold nanoparticles were prepared by the Turkevich method to obtain spherical AuNPs of 80 to 100 nm diameter.[41]

X-Ray Photoelectron Spectrometry (XPS): XPS measurements were performed on modified gold wafer using an ultrahigh vacuum system (Thermo VG Scientific ESCALAB 250). The experiments were performed using a microfocused, monochromatic Al KR X-ray source (1486.6 eV, 650 µm, 15 kVx200 W). The spectra were acquired in the constant analyzer energy mode with pass energies of 150 and 40 eV for the survey and the narrow regions, respectively. Spectra were calibrated by setting the main C1s signal to 285 eV. Surface composition (in at%) was determined using the integrated peak areas and the corresponding sensitivity factors corrected for the analyzer transmission function.

Supporting Information

Supporting Information is available from the Wiley Online Library or from the author.

Acknowledgements

The authors would like to thank Olivier Alévêque and Eric Levillain, who built the spectroelectrochemical measurement setup and developed the data processing software. This work was supported by the ANR-19-CE06-0032.

Conflict of Interest

The authors declare no conflict of interest.

Data Availability Statement

The data that support the findings of this study are available from the corresponding author upon reasonable request.

Keywords

electrografting, organic memristor, spectroelectrochemistry

Received: May 2, 2024
Revised: October 17, 2024
Published online:

[1] Y. Li, Q. Qian, X. Zhu, Y. Li, M. Zhang, J. Li, C. Ma, H. Li, J. Lu, Q. Zhang, *InfoMat* **2020**, *2*, 995.
[2] J.-Y. Shao, B.-B. Cui, J.-H. Tang, Y.-W. Zhong, *Coord. Chem. Rev.* **2019**, *393*, 21.
[3] K. Zhou, Z. Jia, X.-Q. Ma, W. Niu, Y. Zhou, N. Huang, G. Ding, Y. Yan, S.-T. Han, V. A. L. Roy, Y. Zhou, *Int. J. Extrem. Manuf.* **2023**, *5*, 042006.
[4] C. D. S. Dias, P. F. Butzen, *JICS* **2021**, *16*, 1.
[5] G. Ding, J. Zhao, K. Zhou, Q. Zheng, S.-T. Han, X. Peng, Y. Zhou, *Chem. Soc. Rev.* **2023**, *52*, 7071.
[6] J.-H. Tang, T.-G. Sun, J.-Y. Shao, Z.-L. Gong, Y.-W. Zhong, *Chem. Commun.* **2017**, *53*, 11925.
[7] B.-B. Cui, Z. Mao, Y. Chen, Y.-W. Zhong, G. Yu, C. Zhan, J. Yao, *Chem. Sci.* **2015**, *6*, 1308.
[8] S. Goswami, D. Thompson, R. S. Williams, S. Goswami, T. Venkatesan, *Appl. Mater. Today* **2020**, *19*, 100626.
[9] S. Goswami, D. Deb, A. Tempez, M. Chaigneau, S. P. Rath, M. Lal, Ariando, R. S. W., S. Goswami, T. Venkatesan, *Adv. Mater.* **2020**, *32*, 2004370.
[10] A. Bandyopadhyay, S. Sahu, M. Higuchi, *J. Am. Chem. Soc.* **2011**, *133*, 1168.
[11] Q. van Nguyen, U. Tefashe, P. Martin, M. L. D. Rocca, F. Lafolet, P. Lafarge, R. L. McCreery, J.-C. Lacroix, *Adv. Electron. Mater.* **2020**, *6*, 1901416.
[12] S.-J. Liu, P. Wang, Q. Zhao, H.-Y. Yang, J. Wong, H.-B. Sun, X.-C. Dong, W.-P. Lin, W. Huang, *Adv. Mater.* **2012**, *24*, 2901.
[13] S. Goswami, A. J. Matula, S. P. Rath, S. Hedström, S. Saha, M. Annamalai, D. Sengupta, A. Patra, S. Ghosh, H. Jani, S. Sarkar, M. R. Motapothula, C. A. Nijhuis, J. Martin, S. Goswami, V. S. Batista, T. Venkatesan, *Nat. Mater* **2017**, *16*, 1216.
[14] Y. Ma, H.-X. Chen, F. Zhou, H. Li, H. Dong, Y.-Y. Li, Z.-J. Hu, Q.-F. Xu, J.-M. Lu, *Nanoscale* **2015**, *7*, 7659.
[15] S. Sinha, M. Sahad E, R. Mondal, S. Das, L. T. Manamel, P. Brandão, B. de Bruin, B. C. Das, N. D. Paul, *J. Am. Chem. Soc.* **2022**, *114*, 20442.
[16] N. D. Paul, U. Rana, S. Goswami, T. K. Mondal, S. Goswami, *J. Am. Chem. Soc.* **2012**, *134*, 6520.

[17] T.-L. Choi, K.-H. Lee, W.-J. Joo, S. Lee, T.-W. Lee, M. Y. Chae, *J. Am. Chem. Soc.* **2007**, *129*, 9842.
[18] B. Yang, Y. Deng, P. Tao, M. Zhao, W. Zhao, R. Tang, C. Ma, Q. Tan, S. Liu, Q. Zhao, *Org. Electron.* **2020**, *85*, 105815.
[19] T. Menanteau, E. Levillain, T. Breton, *Chem. Mater.* **2013**, *25*, 2905.
[20] A. Laforgue, T. Addou, D. Bélanger, *Langmuir* **2005**, *21*, 6855.
[21] D. Frath, V. Q. Nguyen, F. Lafolet, P. Martin, J.-C. Lacroix, *Chem. Commun.* **2017**, *53*, 10997.
[22] T. Menanteau, S. Dabos-Seignon, E. Levillain, T. Breton, *ChemElectroChem* **2017**, *4*, 278.
[23] J. Lyskawa, D. Bélanger, *Chem. Mater.* **2006**, *18*, 4755.
[24] P. Doppelt, G. Hallais, J. Pinson, F. Podvorica, S. Verneyre, *Chem. Mater.* **2007**, *19*, 4570.
[25] C. Saby, B. Ortiz, G. Y. Champagne, D. Bélanger, *Langmuir* **1997**, *13*, 6805.
[26] P. A. Brooksby, A. J. Downard, *J. Phys. Chem. B* **2005**, *109*, 8791.
[27] P. O. Abate, G. Pourrieux, F. E. Morán Vieyra, M. Cattaneo, M. M. Vergara, N. E. Katz, *Polyhedron* **2018**, *149*, 109.
[28] F. Lebon, R. Cornut, V. Derycke, B. Jousselme, *Electrochim. Acta* **2019**, *318*, 754.
[29] B. Jousselme, G. Bidan, M. Billon, C. Goyer, Y. Kervella, S. Guillerez, E. A. Hamad, C. Goze-Bac, J.-Y. Mevellec, S. Lefrant, *J. Electroanal. Chem.* **2008**, *621*, 277.
[30] I. López, S. Dabos-Seignon, T. Breton, *Langmuir* **2019**, *35*, 11048.
[31] R. Waser, R. Dittmann, G. Staikov, K. Szot, *Adv. Mater.* **2009**, *21*, 2632.
[32] T. Cabaret, L. Fillaud, B. Jousselme, J.-O. Klein, V. Derycke, presented at *14th IEEE Int. Conf. on Nanotechnology*, Toronto, ON, Canada, August **2014**.
[33] S. Mekhmouken, N. Battaglini, G. Mattana, A. Maurin, S. Zrig, B. Piro, D. Capitao, V. Noel, *Electrochem. Commun.* **2021**, *123*, 106918.
[34] L. Pichereau, C. Gautier, T. Breton, *J. Mater. Chem. C* **2022**, *10*, 7111.
[35] P. O. Abate, G. Pourrieux, F. E. Morán Vieyra, C. D. Borsarelli, T. Parella, M. M. Vergara, N. E. Katz, *Polyhedron* **2019**, *174*, 114149.
[36] G. T. Morgan, F. H. Burstall, *J. Chem. Soc.* **1932**, *20*, 30.
[37] A. M. W. Cargill Thompson, *Coord. Chem. Rev.* **1997**, *160*, 1.
[38] H. Casademont, L. Fillaud, X. Lefèvre, B. Jousselme, V. Derycke, *J. Phys. Chem. C* **2016**, *120*, 9506.
[39] K. Bizet, C. Gabrielli, H. Perrot, *Appl. Biochem. Biotechnol.* **2000**, *89*, 139.
[40] O. Alévêque, E. Levillain, L. Sanguinet, *Electrochem. Commun.* **2015**, *51*, 108.
[41] J. Turkevich, P. C. Stevenson, J. Hillier, *Discuss. Faraday Soc.* **1951**, *11*, 55.